Article

Forecasts Plus Assessments of Renewable Generation Performance, the Effect of Earth's Geographic Location on Solar and Wind Generation

César Berna-Escriche [1,2,*] , Lucas Álvarez-Piñeiro [1,2] and David Blanco [1]

1 Instituto Universitario de Ingeniería Energética, Universitat Politècnica de València (UPV), Camino de Vera 14, 46022 Valencia, Spain; lualpi@upv.es (L.Á.-P.); dablade@upv.es (D.B.)
2 Departamento de Estadística, Investigación Operativa Aplicadas y Calidad, Universitat Politècnica de València (UPV), Camino de Vera 14, 46022 Valencia, Spain
* Correspondence: ceberes@iie.upv.es; Tel.: +34-963879245

Featured Application: Applicating stochastic modeling to address the interannual variability and reliability challenges of integrating solar and wind resources into renewable energy systems. The identification of low-production periods emphasizes the importance of storage and generation efficiency, supporting sustainable planning and helping identify ideal deployment locations while adapting to geographical and climatic variations.

Abstract: Solar and wind resources are critical for the global transition to net-zero emission energy systems. However, their variability and unpredictability pose challenges for system reliability, often requiring fossil fuel-based backups or energy storage solutions. The mismatch between renewable energy generation and electricity demand necessitates analytical methods to ensure a reliable transition. Sole reliance on single-year data is insufficient, as it does not account for interannual variability or extreme conditions. This paper explores probabilistic modeling as a solution to more accurately assess renewable energy availability. A 22-year dataset is used to generate synthetic data for solar irradiance, wind speed, and temperature, modeled using statistical probability distributions. Monte Carlo simulations, run 93 times, achieve 95% confidence and confidence levels, providing reliable assessments of renewable energy potential. The analysis finds that during Dunkelflaute periods, in high-solar and high-wind areas, DF events average 20 h in the worst case, while low-resource regions may experience DF periods lasting up to 48 h. Optimal energy mixes for these regions should include 15–20% storage and interconnections to neighboring areas. Therefore, stochastic consideration and geographic differentiation are essential analyses to address these differences and ensure a reliable and resilient renewable energy system.

Keywords: Monte Carlo techniques; uncertainty analysis; climatic regions; earth mapping; electric generation; renewable energy; wind power; solar photovoltaic; Dunkelflaute

1. Introduction

1.1. General Background

Global energy demand has exhibited a consistent upward trend, with a temporary decline in 2020 due to the COVID-19 pandemic, as reported by the IEA in "World Energy Outlook 2023" [1]. Despite the ongoing presence of the pandemic, the upward trajectory in energy demand resumed in 2021 [2]. The reliance on fossil fuels remains predominant, constituting approximately two-thirds of global power generation [3,4]. Achieving economic

decarbonization and net-zero greenhouse gas (GHG) emissions necessitates a comprehensive transition from fossil fuels to renewable energy sources, emphasizing sector-wide electrification and alternative energy solutions where electrification is infeasible [5].

The shift to renewables is imperative due to several interrelated factors. Firstly, renewable energy sources, such as solar, wind, and hydro, offer long-term sustainability compared to finite fossil fuel reserves [6,7]. Secondly, mitigating climate change is critical, as fossil fuel combustion releases substantial GHGs, primarily CO_2 and CH_4, aggravating global warming [8,9]. Transitioning to renewable energy reduces direct GHG emissions, lowering the carbon footprint and minimizing climate-related disruptions. Additionally, reducing fossil fuel use mitigates air pollution, improving public health while renewable technologies become increasingly cost-competitive [10].

Energy supply security is another key driver. Dependence on fossil fuels exposes economies to price volatility, supply chain disruptions, and geopolitical risks, whereas renewable energy enhances energy security and stability [11]. Additionally, this transition fuels technological innovation and advancements within clean energy technologies, leading to economic growth, competitiveness, and job creation [12]. Sustainable economic growth is facilitated as the renewable energy sector stimulates employment in manufacturing, installation, maintenance, and research related to these technologies [13]. Innovation in renewable energy can integrate with energy storage, which often enhances energy efficiency, resulting in optimized energy consumption, reduced waste, and lower energy costs for consumers and businesses [14–16].

International climate commitments, exemplified by the Paris Agreement, underscore the necessity of transitioning to cleaner, more sustainable energy sources. Many nations are committed to reducing carbon emissions and limiting global warming, necessitating a shift towards renewable energy [17,18]. In addition, recent proposals, such as REPowerEU [19], emphasize the urgency of accelerating the transition to clean energy and reducing dependence on imports. Consequently, an integrated approach is needed; then decarbonization entails addressing emissions across diverse sectors, including electricity generation, transportation, industry, and building infrastructure [20,21]. Renewable energies provide a versatile solution applicable to these multifaceted sectors, facilitating a comprehensive transition towards a sustainable, low-carbon future [13,22].

In summary, decarbonizing the economy and achieving net-zero GHG emissions necessitate a systemic transition from fossil fuels to renewable energy, addressing environmental concerns while supporting economic growth, technological progress, and energy security. However, widespread renewable energy adoption presents challenges, primarily due to the inherent variability and intermittency of sources like solar and wind. Fluctuations in sunlight and wind patterns lead to inconsistent energy generation, complicating grid stability and reliability. Unlike conventional power plants, renewables produce electricity only under favorable conditions, requiring solutions to manage supply fluctuations and ensure a stable energy system.

However, large-scale renewable energy deployment presents technical and operational challenges, specifically those related to the decoupling, variability, and unpredictability of the two main renewable sources, i.e., solar and wind power generation [23]. For example, solar energy production invariably peaks during the day, with the maximum in the central daytime hours, which usually does not coincide with electricity demand, usually with significant values during the afternoon-evening. Thus, the need for effective energy storage, demand response mechanisms, or supplementary power sources becomes imperative to bridge this temporal disparity effectively. Additionally, mitigating the consequences of intermittency hinges crucially on developing energy storage systems, most notably batteries, to accumulate surpluses during periods of excess generation for utilization during times of

diminished output. This effort, while indispensable, is fraught with difficult technical and economic challenges, requiring innovation and efficiency improvements.

One of the most remarkable issues arises during Dunkelflauten (DF) events, which refers to extended periods of low solar and wind generation, often worsened by weather conditions such as overcast skies or calm winds. These events pose a serious obstacle to maintaining a reliable energy supply, particularly in regions heavily reliant on renewables. The DF effect highlights the need for supplementary systems such as energy storage, demand response, or complementary power sources to ensure a consistent energy flow during such periods of reduced generation. Addressing these challenges requires innovative solutions in both storage technologies and grid management to mitigate the impact of these extended low-generation events, ensuring energy security even during challenging weather conditions.

Integrating substantial volumes of renewable energy into preexisting power grids exacts an additional challenge on grid infrastructure [10]. Grid operators are compelled to adeptly manage energy flows and sustain stability, particularly when confronted with abrupt fluctuations in renewable generation brought about by meteorological vagaries. The logistical complexities extend to the transmission and distribution of renewable energy, often situated far from densely populated urban centers or regions characterized by heightened demand. The expansion and modernization of transmission and distribution networks are formidable and costly endeavors that are indispensable for efficient energy transport from generation facilities to consumers.

Furthermore, the management of renewable energy centers on precise production forecasts [24,25]. The inherent fluctuations in solar and wind generation mandate deploying sophisticated forecasting techniques to ensure grid stability and a reliable energy supply. Geographical considerations also exert a profound influence on renewable energy feasibility. The uneven distribution of renewable resources across regions necessitates meticulous planning to optimize the siting of renewable energy projects, striking a balance between resource abundance and proximity to demand centers. The regulatory landscape presents yet another layer of complexity, with policies and regulations often misaligned with the unique characteristics of renewable energy generation. Establishing supportive frameworks that incentivize investment, grid integration, and innovation is paramount in surmounting these challenges.

1.2. Characterizing Renewable Generation Across Climate Zones

The Köppen–Geiger climate classification system has long served as a foundational framework for categorizing global climates based on temperature and precipitation patterns [26]. Integrating Hybrid Renewable Energy Systems (HRES) across diverse Köppen–Geiger climate zones presents a significant opportunity to optimize techno-economic performance in standalone and grid-connected applications. The methodology for mapping and optimizing these systems involves a comprehensive analysis of local climatic conditions, resource availability, and economic factors, which can vary dramatically across different geographical regions. Mazzeo et al. [27] studied the energy reliability and economic profitability of optimal PV-wind HRES in standalone and grid-connected systems considering 48 different locations from the Köppen–Geiger climate zones. However, this classification only considers temperature and precipitation, while the second and third-letter classifications provide limited relevance for photovoltaic (PV) applications.

However, as the classification is based on temperature and precipitations is not well suited for energetic purposes. Recently, this classification has been adapted to better serve the photovoltaic (PV) sector by developing the Köppen–Geiger-photovoltaic (KGPV) classification. This innovative approach integrates solar irradiance as a critical factor

influencing PV system performance, thereby enhancing the utility of the Köppen–Geiger framework for assessing solar energy potential across different climatic zones [28].

Finally, large-scale renewable energy projects can raise environmental and land-planning issues, particularly in ecologically sensitive areas or locales with competing land-use priorities [10]. Addressing these concerns necessitates a comprehensive and judicious approach to project development and environmental stewardship.

In summary, although highly advantageous in sustainability and mitigating environmental impacts, adopting renewable energy sources presents a complex array of challenges linked to the variability of energy generation and its implications for effective energy management. Solving these multifaceted challenges necessitates innovative solutions across various domains, including energy storage, grid orchestration, transmission infrastructure enhancement, and establishing policy frameworks that underpin a dependable and resilient transition to renewable energy sources.

Remarkably, the location-specific nature of these challenges emphasizes the importance of context-aware strategies to harness the potential of renewable resources efficiently. A pivotal factor in this context is the influence of latitude, which substantially dictates the availability and characteristics of solar and wind resources within a given geographical region. The energy derived from solar and wind sources arises from the intricate interactions involving the Earth, the sun, and the atmosphere, and these interactions exhibit latitude-dependent variations due to the Earth's axial tilt and its rotational dynamics [29].

Solar energy experiences notable variations in its availability dictated by latitude, driven primarily by the angle at which sunlight strikes the Earth's surface. Therefore, several aspects affecting this resource need to be considered:

- Solar Insolation: Lower latitudes receive higher solar insolation due to direct sunlight, whereas higher latitudes experience reduced insolation as sunlight strikes at shallower angles.
- Daylight Duration: High-latitude regions have extended daylight in summer but shorter daylight in winter, impacting solar energy generation.
- Seasonal Variation: Seasonal fluctuations in solar energy are more pronounced at higher latitudes due to the Earth's axial tilt, while equatorial regions experience minimal variation.

Wind energy is generated by the movement of air masses driven by the uneven heating of the Earth's surface, being influenced by latitude-dependent factors:

- Coriolis Effect: Wind patterns strengthen with latitude due to the Coriolis effect, leading to more robust and consistent winds at higher latitudes.
- Pressure Gradients: Temperature differences between equatorial and polar regions create pressure gradients, driving large-scale wind systems like trade winds and westerlies.
- Topography: Coastal and mountainous areas influence wind patterns, often intensifying wind speeds and creating localized high-potential wind zones.

Then, the interaction of latitude-dependent factors significantly influences the availability and characteristics of solar and wind resources. Optimizing renewable energy use requires adapted approaches that consider these variations. Based on these differences, the Earth can be categorized into three major regions with distinct implications for renewable energy generation:

- Equatorial Regions: High and consistent solar radiation makes solar energy the dominant option, while wind resources are generally weaker.

- Mid-Latitude Regions: Balanced potential for both solar and wind energy, with wind resources offering reliability.
- High-Latitude Regions: Lower solar potential due to oblique sunlight and short daylight hours, but strong and consistent wind resources make wind energy a preferable choice.

In conclusion, latitude plays a crucial role in shaping solar and wind energy potential, with equatorial regions favoring solar energy, mid-latitudes offering a balance, and high-latitude regions benefiting from strong wind resources. However, other factors, such as proximity to the coast, topography, and aridity, also significantly influence renewable energy generation, necessitating comprehensive planning for optimal efficiency and sustainability [23]. Figure 1 displays Earth's maps showing the irradiance and average wind speed at 50 m. Therefore, at a first attempt, Earth's regions can be categorized based on their capability to produce electricity from wind and solar resources. If detailed information on the existing resources in each region of the Earth is desired, NASA's POWER Data Access Viewer database [30] can be consulted. However, in this study, an in-depth analysis of solar and wind resource capabilities has been carried out by taking nine specific locations that characterize the nine combinations of solar and wind resources cited above.

This classification provides a general framework but may not account for all regional variations. However, to offer a broad understanding of generation capacities, the Earth's regions are categorized into nine groups, as outlined in Table 1.

Once the main regions of the Earth have been identified based on their solar and wind resources, the next step involves quantifying these resources in a representative area of each identified region. This process enables a deeper understanding of the magnitude and variability of available resources in each area, laying the groundwork for evaluating the electrical generation capacities through renewable sources. Databases containing detailed information on solar and wind resources worldwide are employed to accomplish this task. These databases compile historical and real-time data on solar radiation, wind speed and direction, and other relevant climatic parameters. Following the acquisition of these databases, the next step involves characterizing the behavior of solar and wind resources throughout the year in each area of interest, i.e., identifying each variable's probability density functions (PDFs). This includes analyzing seasonal, daily, and hourly solar radiation and wind variability and identifying climatic patterns and atmospheric phenomena that may influence resource availability. Subsequently, specific procedures are employed to calculate each area's potential for renewable energy production. This involves utilizing mathematical models and simulation algorithms that mainly integrate climatic data and technical parameters of renewable generation systems such as solar panels and wind turbines. This process provides the necessary information to make informed decisions regarding the development of renewable energy projects and the planning of sustainable energy infrastructures on a global scale.

In pursuit of these objectives, the paper is organized as follows: Section 2 provides an approach to renewable generation sources and the procedure to estimate electric generation. Section 3 focuses on showing the results of the forecasted scenarios and describes and analyzes the major findings related to the energy generation scenarios. Finally, Section 4 is dedicated to summarizing the conclusions of the current study regarding the generation systems performance depending on the locations of the generation systems. Additionally, some possible future work is also mentioned in this section.

(**a**)

(**b**)
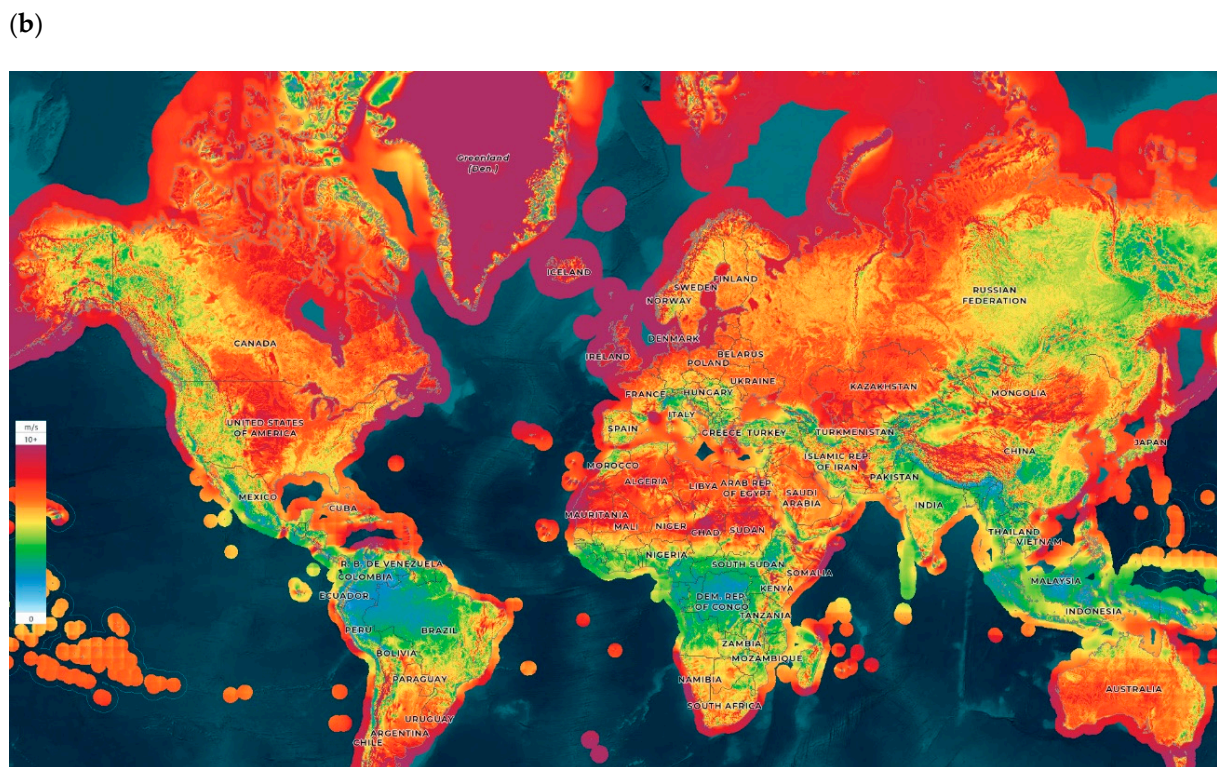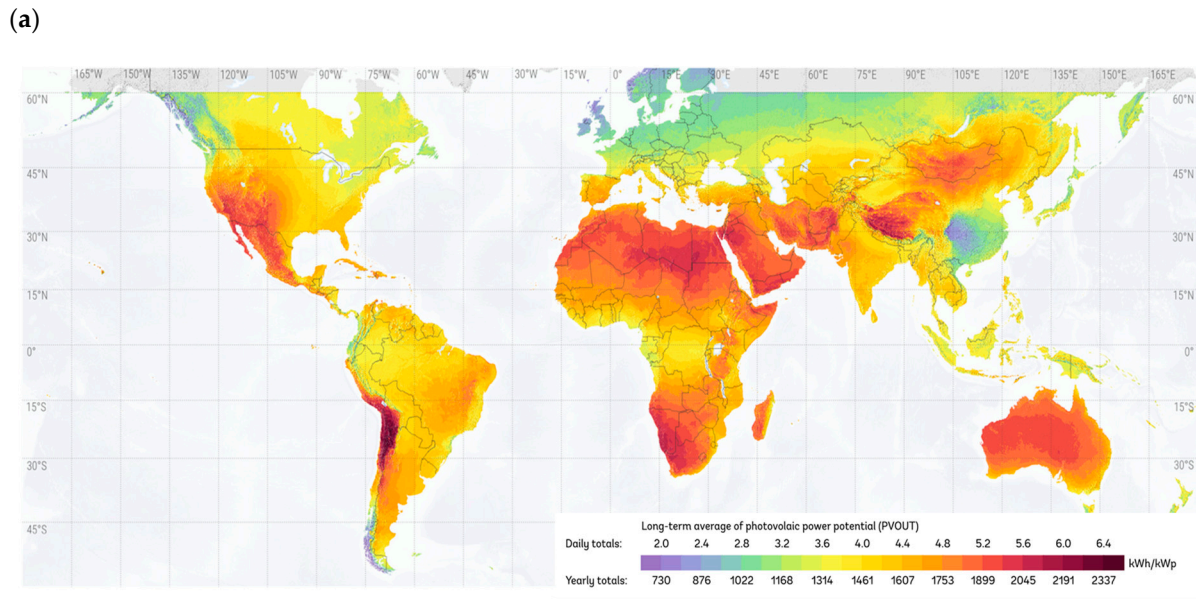
Figure 1. Color maps of the Earth's natural resources: (**a**) Sun; (**b**) wind. (Based on the NASA POWER Data Access Viewer [30]).

Table 1. Solar and wind resource classification.

Region Group	Characteristics	Example Regions
1. High solar and wind (HS-HW)	- High solar insolation - Strong wind resources - Ideal for both solar and wind energy	- Southern Australia - Southern Africa - Coastal Sahara Desert - South America - Islands and coastal mid-latitudes

Table 1. *Cont.*

Region Group	Characteristics	Example Regions
2. High solar and moderate wind (HS-MW)	- Very high solar insolation - Moderate wind resources - Desertic/semi-desertic areas	- Sahara Desert (Africa) - Atacama Desert (South America) - Arabian Desert (Asia) - Southern USA - Northern Mexico - Southern Spain
3. High solar and low wind (HS-LW)	- High solar insolation - Weak wind resources due to Coriolis effect	- Ecuador - Colombia - Indonesia
4. Moderate solar and high wind (MS-HW)	- Strong, consistent winds - Moderate sunlight - Suitable for wind energy projects	- Scotland - Ireland - Denmark - Nova Scotia (Canada)
5. Moderate solar and wind (MS-MW)	- Moderate solar insolation - Consistent wind resources - Suitable for mixed energy projects	- South Africa - USA - China - Central European countries
6. Moderate solar and low wind (MS-LW)	- Moderate solar insolation - Weak winds - Challenging conditions for renewable energy generation	- Central Valley (California) - Inner Mongolia - Turkmenistan - Kyrgyzstan
7. Low solar and high wind (LS-HW)	- Strong wind resources - Low solar radiation - Suitable for wind energy projects	- Northern Canada - Patagonia (Argentina) - Russia - Northern Scandinavia
8. Low solar and moderate wind (LS-MW)	- Low solar potential - Moderate wind resources - Suitable for small-scale wind projects	- Pacific Northwest (USA and Canada) - Inland Western Europe - Northern Japan
9. Low solar and low wind (LS-LW)	- Low solar and wind resources - Major challenges for renewable energy generation	- Northern Siberia - Greenland - British Columbia (Canada)

2. Characterization of Wind-Solar Power Generation for Earth Regions

In the field of renewable energy generation planning, a fundamental aspect involves examining the generation characteristics associated with the unpredictability and variability inherently linked to the two resources that currently, as well as at least in the near future, constitute the majority of renewable generation, namely solar photovoltaic and wind generation. The current analysis delves into the electric power generation capabilities from solar photovoltaic and wind technologies, focusing on the main groups of environmental conditions found on Earth. Thus, the initial objective of characterizing the resources and generation for each technology within each of the regions defined throughout the year will be presented below, followed by the characterization of the generation technologies required to take advantage of these resources and then describing the tool needed to establish how to take advantage of the available resources through the associated technologies, i.e., the curves that characterize the performance of the generation equipment used. That is, the power curves of the generation equipment (standard curves of conventional commercial models have been taken) are coupled with the wind and solar resources (plus temperatures, since they affect the performance of the solar panels). For the estimation of the existing renewable resources, 10 years of the above-mentioned databases have been analyzed to

characterize the PDFs (probability density functions) followed by these resources. In order to achieve the other main objective of this work, the comparison of solar and wind generation performance variations according to the different climatic characteristics that determine the performance of solar panels and wind turbines.

In this regard, and to carry out these analyses, it is necessary to consider and analyze in detail primarily the following three aspects:

1. Estimation of renewable resources: To support this analysis, historical datasets of wind and solar resources for the different climatic regions under consideration are compiled to estimate the resources available for each of the main environmental conditions on Earth. This provides patterns on the availability of these renewable sources under specified conditions. Accurate characterization of solar irradiance and wind speed patterns in various geographic zones is vital for estimating energy generation potential and identifying suitable locations for renewable installations. Therefore, a section has been dedicated to the complexities of our data sources and methodologies that underpin the assessment of solar and wind resources.

2. Characterization of the renewable generation system: Typical performance values of the generation systems considered within this study have been taken. It is important to note that it has been assumed that there are no significant disparities in performance between different current commercial models, so typical characteristics have been assumed for solar PV and wind generation. Specifically, a conventional wind turbine and standard photovoltaic solar panels have been used in current simulations, acknowledging their suitability in renewable energy projects worldwide. Renewable energy, namely solar and wind sources, is a cornerstone of contemporary energy strategies. This document comprehensively evaluates the technical specifications, efficiency metrics, and maintenance requirements associated with the solar and wind generation equipment used in our analyses. These details are crucial for assessing renewable energy sources' performance and seamless integration into the broader energy grid.

3. Finally, it is essential to analyze the differences between different climates, considering their annual generation capacity for resources in all climate regions and the peculiarities over the different timeframes. Thus, to estimate the strengths and weaknesses of each resource for the different regions and during the different phases of the year, especially paying attention to Dunkelflauten (DF) periods. The DF phenomenon is well known in countries or regions that rely on energy mixes and is heavily comprised of wind and solar power. Ambitious energy transitions to more renewable energy have made these periods a critical challenge, for example, in Germany in the last few years. Since the decommissioning of nuclear power, this country has suffered peaks in energy prices and relied more on fossil fuels, especially during winter [31].

The following subsections will discuss how data on available solar and wind resources are collected and, secondly, how the potential generation for each defined climatic region is estimated. This calculation will not only be conducted on an annual basis but also across various temporal intervals for further analysis.

2.1. The Renewable Resources

In prospective net-zero emissions energy systems, solar and wind resources will assume a predominant role; the potential emergence of spatial and temporal misalignments between the availability of these resources and the temporal patterns of electricity demand poses a substantial challenge to the overall reliability of the energy system.

Historical data from a specific year are often used to reflect or estimate annual solar and wind power production. However, relying on data from just one year does not capture all the various aspects and characteristics of an energy system [32]. Initially, a deterministic model or scenario creates a mathematical representation where identical inputs or initial conditions invariably yield consistent outputs, disregarding randomness or uncertainty in the modeled process. However, different reference years can lead to differing probabilistic outcomes, with a standard year being more likely to occur than extreme years. Employing a probabilistic, stochastic, or non-deterministic model in a second phase seeks to quantify the uncertainty associated with the variable(s) under investigation.

The uncertainty associated with renewable energy sources has been extensively analyzed using Monte Carlo analysis (MCA). The MCA entails conducting numerous simulations with random variations in uncertain input. Typically, PDFs are used for this propagation since not all possible values are feasible or realistic (for example, negative wind speeds, negative solar irradiance, or freezing temperatures in typically warm regions might not be adequate). Each assigned PDF is executed multiple times using a single set of inputs for each run. The number of runs can vary from hundreds to several hundred, but it can also be determined statistically. According to Wilks' formula [33,34] and Wald's extended expression of applicability to multivariate distributions [35], 93 runs that ensure a 95% probability of falling within a two-sided 95% confidence interval have to be run. Although this approach originates within the safety margins of the nuclear sector [36], it has found its application in the uncertainty analysis of energy sources [37–39].

Leveraging the POWER Data Access Viewer database from NASA [30], this study analyzes the solar and wind resource capacities of nine sites relevant to Earth's climate classification. These nine scenarios have been selected to include a comprehensive range of solar and wind resource magnitudes, effectively characterizing the primary terrestrial regions. Within each of these scenarios, solar and wind generation composition has been systematically estimated to ascertain the generation at each location and at any time over the whole Earth. Consequently, each scenario determines the generation at each geographical location over the year.

The probabilistic nature of this time series is used to create synthetic datasets for a robust analysis. The statistical properties of solar irradiance, wind speed, and ambient temperature are determined using historical data from the NASA POWER Access Viewer [30] and other sources such as PVGIS [40].

Figure 2 illustrates steps to create the synthetic wind, solar, and temperature hourly data. The approach employed follows the steps of Berna-Escriche et al. [39] and Álvarez-Piñeiro et al. [38]. Having in mind the considered confidence and coverage and the availability of climatic data, firstly, the PDFs that best fit the observed data are identified using hourly values recorded from 2001 to 2023.

The historical data are normalized against the weekly maximum values to obtain an auxiliary parameter, k_i, used to generate synthetic data. This normalization removes seasonal effects and ensures the data fit within a common range for better comparison and analysis. Each week has a specific PDF associated with it. The auxiliary parameter being defined as:
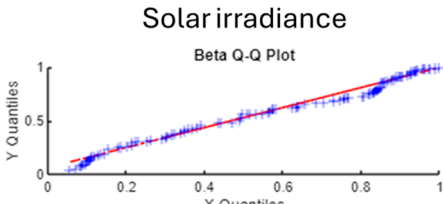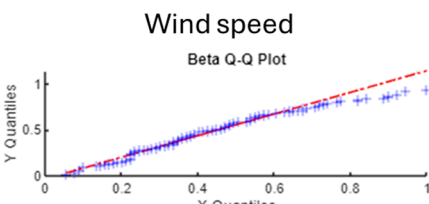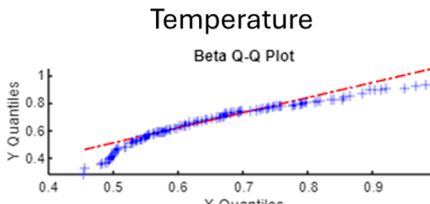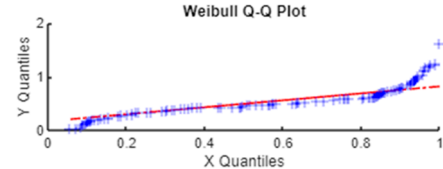
$$k_i = \frac{x_i}{\max(x_{week,i})} \tag{1}$$

From the literature, solar irradiance data are best represented with a beta distribution [41], wind speed by Weibull [42]. At the same time, ambient temperature finds its best distribution by normal distribution [43]. So, these three distributions were evaluated.
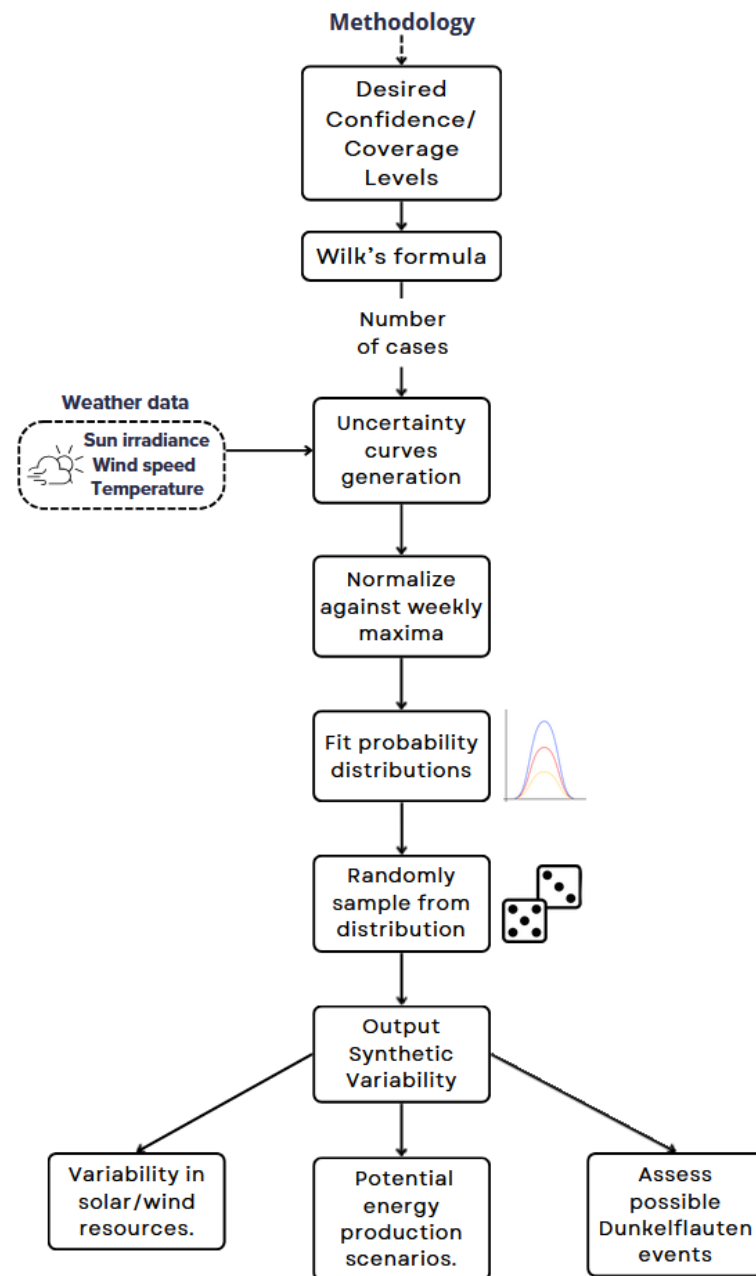
Figure 2. Summary of the main steps to be followed in applying the BEPU methodology.

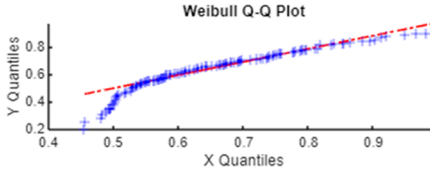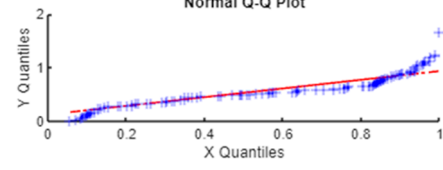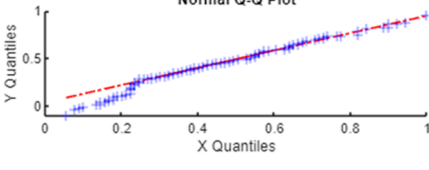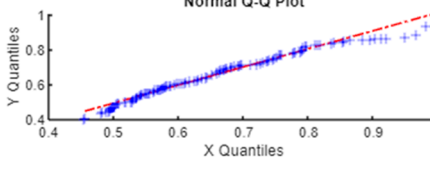After estimating the parameters of the distributions using the maximum likelihood method (MLE) via the fitdist function in MATLAB (MatLab R2023a), a comprehensive assessment of the fit and goodness of fit for each variable (solar irradiance, wind speed, and temperature) was conducted, as summarized in Table 2. The Akaike information criterion (AIC) and Bayesian information criterion (BIC) for each fitted distribution were calculated to validate the choice of probability distributions. These criteria were used to compare the selected models (Beta, Weibull, and normal). The chosen models consistently demonstrated lower AIC and BIC values, confirming their suitability for representing the observed data, with the best fits being the beta distribution for solar irradiance, the Weibull distribution for wind speed, and the normal distribution for temperature.

Table 2. Summary of the best-fit distributions for solar, wind, and temperature resources.

Solar irradiance	Wind speed	Temperature
AIC values;	AIC values;	AIC values;
Beta: −11.8591	Beta: −32.3662	Beta: −134.8166
Weibull: 73.6683	Weibull: −41.2643	Weibull: −158.4579
Normal: 73.7159	Normal: −32.6231	Normal: −172.264
BIC values:	BIC values:	BIC values:
Beta: −6.0935	Beta: −26.6006	Beta: −129.0359
Weibull: 79.4339	Weibull: −35.4987	Weibull: −152.6772
Normal: 79.4815	Normal: −26.8575	Normal: −166.4833

Once the PDFs are fitted to the historical data, the synthetic datasets are generated by randomly sampling from these distributions. A random parameter k_i is selected and applied consistently across all 52 weeks of the year from the fitted PDFs, multiplied by the maximum registered value for each week across the complete dataset from 2001 to 2023. Finally, a synthetic dataset that spans 8760 h, representing the availability of renewable sources, is obtained. This process can be repeated the desired number of times, such as the number of runs or assessments. As mentioned before, Wilk's formula yields a number of 93.

This artificial dataset accurately simulates the variability and probability of renewable energy sources. It preserves the statistical properties of historical data, including mean, variance, and distribution shape. By incorporating stochastic elements, the approach reflects the unpredictable nature of renewable energy generation, enabling a robust evaluation by simulating a wide range of potential scenarios.

In Figure 3, the synthetic curves illustrate the natural intermittency and variability of renewable energy sources, particularly solar irradiance and wind speed, represented in blue. While a deterministic approach can assess renewable energy availability over a year—using registered values and/or historical data, depicted in red in Figure 3—incorporating multiple scenarios for wind speed, solar irradiance, and temperature enables a more comprehensive analysis. This probabilistic approach considers a wider range of possibilities, offering a complete understanding of the variability and uncertainty associated with renewable energy generation.
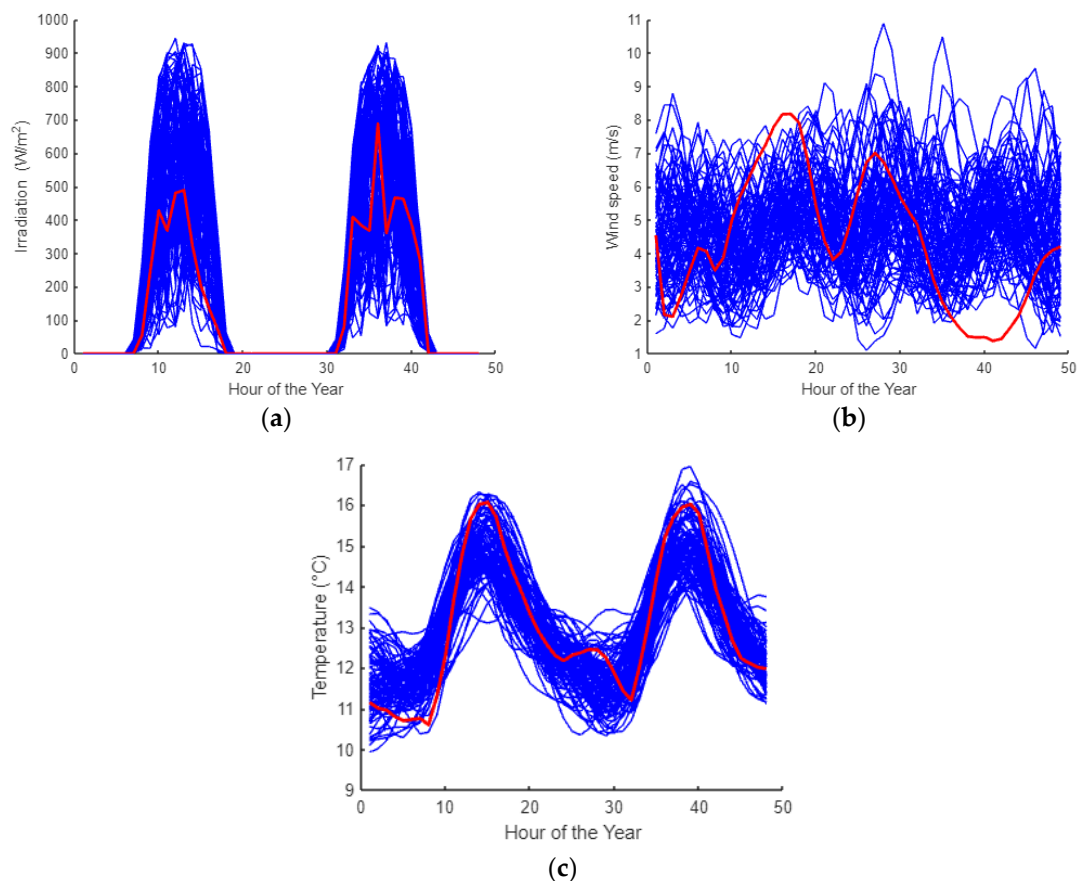
Figure 3. Extraction of two days generated (**a**) irradiance, (**b**) wind speed, and (**c**) synthetic curves for temperature. In red is one of the historical registered values (year 2001) for comparison.

2.2. The Renewable Power System

Solar and wind power generation systems have proven to be significant generation resources. Still, their random nature, variability, intermittency, and geographical limitations make the analyses associated with their production capacities complex. Therefore, predicting the generation capacities becomes important once the existing resources are estimated. To this end, the main considerations taken for estimating the generation capacities of these systems are detailed below.

Solar PV technology offers the potential to convert sunlight into electricity directly, yet its performance still falls short of desired levels, prompting ongoing scientific and engineering focus. Solar radiation, wind speed, temperature, humidity, and dust influence PV panel efficiency, which remains central to energy system reliability and economic viability. However, predicting power output is complex due to the non-deterministic relationship between PV production and variable environmental conditions. Regression, statistical analysis, and machine learning are commonly employed to address forecasting challenges. Recent advancements in machine learning, data science, and artificial neural networks are increasingly utilized to improve accuracy in predicting PV power generation [44].

To construct a model that accurately predicts the electrical production that a given type of solar panel can achieve once the PDFs followed by the existing environmental conditions in each analyzed region are known, it is necessary to have a predictive model. Such a model can be obtained from experimental data on panel performance and, from there, using one of the techniques to reach the desired model. That is, data preprocessing is first carried out, then input variables affecting panel electrical generation are selected; in

this case, solar irradiation, ambient, and module temperature are set as the objective. Other variables may have an effect, such as wind speed and humidity [45].

The generated power of a PV panel depends on the cell efficiency, the panel's efficiency, its area, and the sun irradiance:

$$PPV = \eta_{cell} \cdot \eta_{panel} \cdot A \cdot G \tag{2}$$

A linear model is used as a simplified version of the proposed model by Duffie and Beckman [44]. Solar panel performance relies on solar radiation and temperature. As Duffie and Beckman [44] propose, the cell efficiency depends on the temperature, and the cell temperature depends on its efficiency. This iterative process is simplified by using a correction coefficient for the most common crystalline silicon-based applications [46,47]:

$$\eta_{panel} = \eta_{ref} \cdot \left(1 - \beta \cdot \left(T_c - T_{ref} \right) \right) \tag{3}$$

where η_{ref} is the reference efficiency of the solar panel, β is the correction coefficient, T_c is the solar cell temperature, and T_{ref} is the temperature of reference. The correction for temperature changes reflects how cell efficiency affects the overall panel performance.

The solar panel temperature T_c is determined by a linear formula that considers the ambient temperature and the solar irradiation by:

$$T_c = T_a + \left(\frac{G}{G_{NOCT}} \right) \cdot (T_{NOCT} - 20) \tag{4}$$

where T_a is the ambient temperature (°C), T_{NOCT} is the nominal cell operating temperature (°C), G is the measured solar radiation intensity (W/m^2), and G_{NOCT} is 800 W/m^2.

$$PPV = P_M \cdot \left(\frac{I}{I_{STC}} \right) \cdot \eta_{panel} \tag{5}$$

where P_M is the maximum rated power output power in standard conditions, and I_{STC} is the solar irradiance in standard conditions.

Thus, the achieved electrical generation can be estimated based on Equation (4) and the data of the atmospheric variables mentioned above (Section 2.1). However, not only can this be estimated deterministically, but it is also possible to estimate generation ranges by analyzing the PDFs followed by the different variables appearing in Equation (4). In other words, it is possible to use one of the various statistical uncertainty propagation techniques to estimate confidence intervals of electrical generation over the desired time period.

In relation to wind generation, in the field, the power output of wind turbines usually deviates to some extent from the rated power curve presented in the equation below [48]:

$$P_T = \frac{1}{2} \cdot \rho \cdot A \cdot W^3 \cdot c_p \tag{6}$$

where ρ is air density, A the area swept by a turbine's rotor, W the wind speed and c_p the power coefficient.

Wind speed is obtained in some databases at specific heights, such as 10 or 50 m [30]. The wind speed at different heights, such as at a specific hub height that differs from the provided height, can be estimated using the Hellman exponent g, which ranges from 0.1 to

0.4. This range depends on surface roughness and atmospheric conditions, and the wind speed estimation can be made through exponential extrapolation:

$$W_h = W_{ref} \cdot \left(\frac{H}{H_{ref}} \right)^g \tag{7}$$

The power output of the wind turbine is determined using its turbine characteristic power curve, which depends mainly on the wind speed at hub height. These characteristic curves relate the wind speed with the power produced. However, three main speed ranges need to be taken into account:

$$
\begin{aligned}
P_T &= 0 \quad \text{if } W \le W_{LC} \\
P_T &= \tfrac{1}{2} \cdot \rho \cdot A \cdot W^3 \cdot c_p \quad \text{if } W_{LC} < W < W_{UC} \\
P_T &= 0 \quad \text{if } W \ge W_{UC}
\end{aligned}
\tag{8}
$$

When the wind speed is less than or equal to the lower cutoff wind speed W_{LC}, there is no generated power. The same occurs when the wind speed is above the upper cutoff wind speed W_{UC}. This occurs up to the upper cutoff, after which the turbine stops or reduces its power output to protect itself.

Other issues, such as the air density variations ρ, for example, play a significant role. There are widely adopted international regulations to analyze these influences, which describe simple, physics-informed methods to account for these effects. Furthermore, there are technical reasons affecting the performance of the wind turbine, namely intended or unintended deviations from the optimal control scheme and, therefore, the optimal value of c_p or power coefficient, which can lead to deviations from the standard power curve [48]. In any case, c_p can be estimated from the wind generator's power curve versus wind speed [48]. Its value is estimated from models, calculated using an exponential relationship that accounts for rotor dynamics and control settings, by the tip-speed ratio λ and β, which is the pitch angle of the blades [48]:

$$
\begin{aligned}
c_p(\lambda, \beta) &= c_1 \left(\tfrac{c_2}{\lambda} - c_3 \beta - c_4 \beta^{c_5} - c_6 \right) \exp\left(-\tfrac{c_7}{\lambda} \right) + c_8 \lambda \\
\lambda &= \tfrac{r\omega}{W}
\end{aligned}
\tag{9}
$$

where ω is the rotor's angular speed and r is the blade's length. The value of β is set to zero to get the maximum power extraction and the optimum λ is considered [49].

The wind generation is estimated with the previous equations and the uncertainty in its production is forwarded by the wind speed, as mentioned before with the crafting of synthetic wind speed curves and by the different constants c_i (Table 3). Typical values for these constants are taken from Bustos et al. [50,51], and an uncertain range of $\pm 10\%$ is employed, allowing for deviations, atmospheric and working conditions, and other possible factors.

Table 3. Summary of the main coefficient's values used for windmill calculations.

c_1	0.44
c_2	124.99
c_3	0
c_4	2.2
c_5	21
c_6	18.4

As with solar photovoltaic generation, it is possible to provide wind turbine power generation over time, with confidence intervals for the generation and different periods. In this case, the uncertainties associated with the terms in Equation (6) must be propagated.

3. Results and Discussion

To obtain consistent results, several considerations must be kept in mind. First, the regions should be characterized by obtaining climatic and geographical data to differentiate between areas with higher and lower solar and wind potential. Next, uncertainties need to be estimated by quantifying the variabilities associated with solar and wind resources and those related to the power generation systems, such as the efficiency of solar panels and wind turbines. Then, these uncertainties must be propagated by applying statistical methods and uncertainty propagation models to calculate how uncertainties in solar and wind resources affect total electricity generation. To carry out the uncertainty propagation, as advanced mainly in the introduction and methodological sections, BEPU techniques in advanced energy scenario predictions have been used. In particular, using Wilks' formula and stochastic approaches for the energy generation calculations. Finally, the annual, monthly, and daily electricity generation from solar and wind energy in each region should be characterized, including identifying low-generation periods and comparing the advantages of solar versus wind in each area. Additionally, the complementarity between solar and wind resources should be analyzed to enhance the stability of the generation system.

Consequently, the section is divided into three subsections. The first subsection describes the resources in each earth's zone. Next, the second one presents the outcomes of applying the methodology to the deterministic base scenario, revealing the results of the 93 simulations. Finally, the third subsection elucidates the principal results and findings obtained by comparing the performance of the analyzed condition.

3.1. Characterization of Solar and Wind Resources in the Earth's Regions

As mentioned above, the first step is to characterize both the wind and solar resources in the different areas to be considered. Thus, in order to provide an idea of the behavior of each zone for both resources, Figures 4 and 5 display the histograms of the historical hourly data for more than 20 years of data used. To remind that from the actual historical data of each location, their PDFs have been estimated, and from them, a Monte Carlo methodology has been used based on the Wilks formula. The result has been a random sampling; in the case of the analysis as explained in Section 2.1, there are 93 random samples, so that from them the hourly behavior of solar and wind resources at 95% confidence and coverage levels has been estimated.

Beginning with wind characterization, as shown in Figure 4-1, areas of high wind exhibit annual average speeds consistently in the range of 8–10 m/s. Notably, these regions experience sustained winds, with 50% of the time featuring wind speeds between 5–7 m/s and 11–12 m/s. Regarding the coastal Sahara region specifically, it has sustained wind speeds from approximately 5 to 14 m/s for around 50% of the time, with a very symmetrical probability density function (PDF). The other two high wind speed locations show more significant variability and exhibit slight positive skewness, with winds 50% of the time in the range of just over 5 m/s to 11–15 m/s. Additionally, both locations occasionally experience mean wind speeds exceeding 20 m/s, reaching 30 m/s.
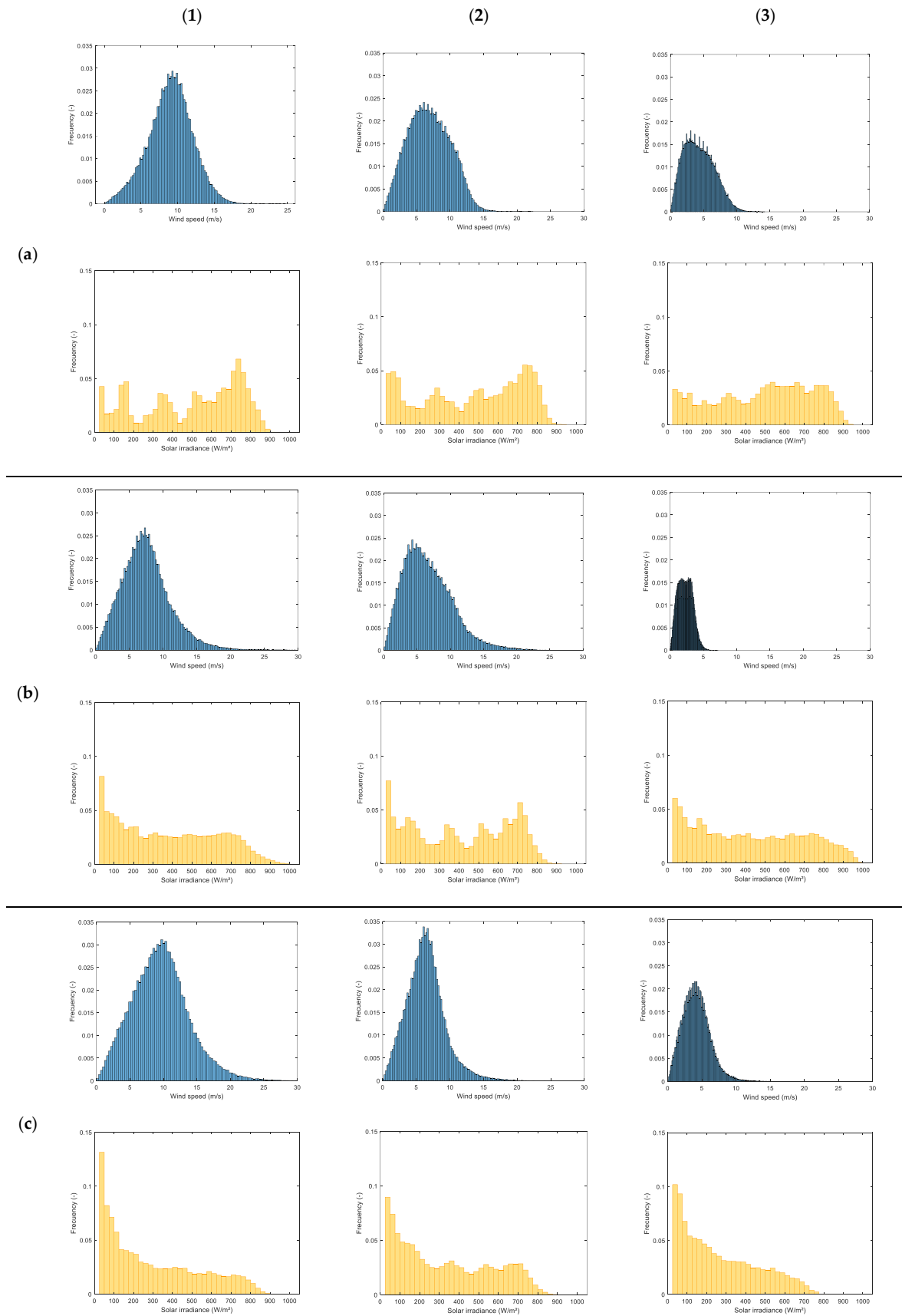
Figure 4. Histograms of the hourly wind and solar resources for the nine terrestrial locations considered, (**a–c**) solar irradiance: high, moderate and low; (**1–3**) wind speed: high, moderate, and low.
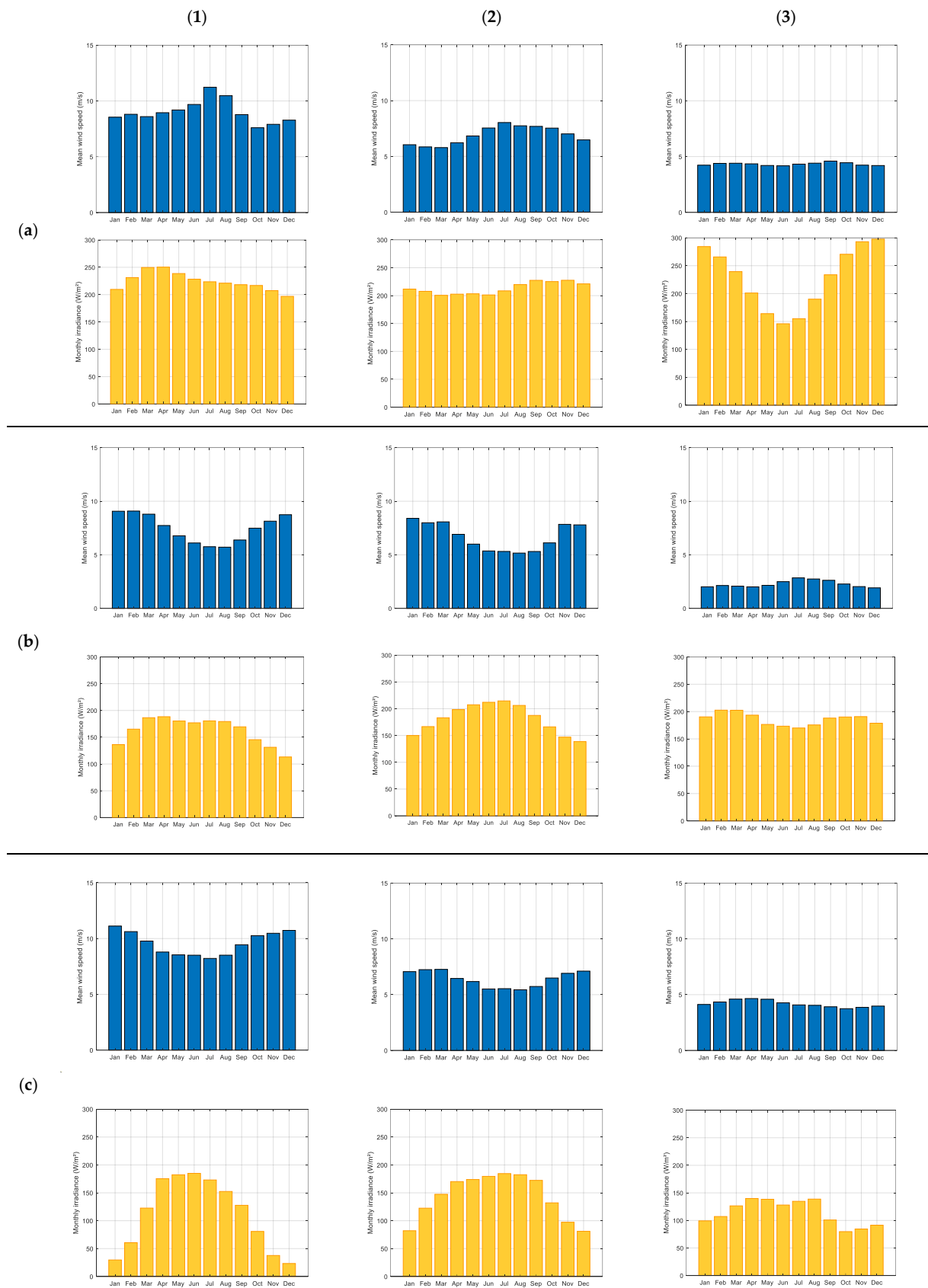
Figure 5. Monthly average values of the hourly wind and solar resources for the nine terrestrial locations considered: (**a**–**c**) solar irradiance: high, moderate, and low; (**1**–**3**) wind speed: high, moderate, and low.

Regions with moderate wind (Figure 4-2) exhibit annual average speeds around 6–7 m/s, with 50% of the time featuring wind speeds between 3–4 m/s and 8–10 m/s. All three regions display positively skewed distributions, particularly the last two. Especially the second one, which with a certain regularity passes the 15 m/s and occasionally the 20 m/s.

Low wind regions (Figure 4c) demonstrate annual average speeds around 3–5 m/s, with wind speeds 50% of the time between 2–3 m/s and 5–7 m/s. Their distributions are positively skewed, with no significant occurrence of wind speeds above 5–10 m/s. Specifically, the Kindu area (in the center of Africa), which has almost no average hourly speeds over 5 m/s. However, the Antofagasta and Chengdu regions exhibit some hours with wind speeds between 10 and 15 m/s, though such instances are quite rare and do not lead to significant generation. These regions are generally dominated by extended periods with almost no wind activity.

Regarding solar irradiance characterization, the data for the high irradiance regions (Figure 4a) show that values around 500–900 W/m^2 are the dominant intervals. Regions with moderate irradiance have significant contributions around 500–900 W/m^2, but also with important percentages in the lower irradiance ranges (Figure 4b). While low-resource areas (Figure 4c) make the most significant contributions in the lower range, close to zero and even reach lower maximum irradiance values. All this added to a lower number of total hours of sunshine per year. And that for the first group there are a total of approximately 4700 h per year, for the second group about 4500, and for the third group about 4300.

If the focus is now on the monthly allocations (remember that in spite of showing these monthly mean values, the analyses are really hourly but are shown in this way to show only the general differences in their characteristics), certain patterns can be appreciated. For example, the wind has generally higher values in the winter months, and for the high and moderate wind regions, this difference is clearly seen (Figure 5). In the high wind regions (Figure 5-1), the mean summer values are appreciably lower than the winter values, ranging, respectively, from 5.5 to 9.5 for the Massachusetts region (Figure 5(b1)) and 8.5 to more than 10 for the North Sea area (Figure 5(c1)), while for the Sahara coastal region (Figure 5(a1)), the trend is the opposite (mean values even above 10 m/s in the summer months and down to 8 in autumn-winter). While for the low wind regions (Figure 5-3), this difference is not very appreciable, given its small magnitude.

In the case of irradiance, the situation is similar, with generally a clear difference between summer and winter, in this case the situation is more pronounced in the locations with greater longitudes. Although in the regions of high irradiation (Figure 5a), this difference is not seen, with high values all year round, except in the area of Antofagasta (Chilean Andes), where there is a very clear seasonality (Figure 5(a3)), the high irradiation comes from its low latitude, but also because of its high altitude, in this case, it has a very pronounced seasonality (located in the southern hemisphere, so the highest irradiances are between October and February). There is a greater seasonality for the moderate and low irradiation values, especially in the location with the highest latitude, the North Sea area, despite its lower average values (Figure 5(c1)).

*3.2. Propagation of Uncertain Input Variables to Estimate the Electric Generation*

As described in Section 2.1, based on the data described in the previous section, random sampling of the resources has been carried out, so that the generation is determined based on the characteristics of the solar panels and wind turbines, described in Section 2.2. A unitary power of 1 MW has been considered for both solar and wind installations. As summarized in Figure 6, there is a baseline behavior around which sampling variations

occur; for instance, wind power generation is about 240 MWh during the month of March, with most of the 93 random sampling scenarios in the range of 210 to 270 MWh.
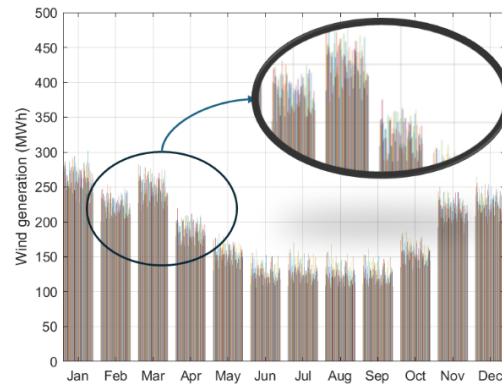

Figure 6. Random sampling behavior for monthly wind generation in the Mediterranean Region.

Focusing the analysis on the generations, as summarized in Figures 7 and 8, the 93 samples of the monthly average values for both resources and for all locations are shown. Remember that although the monthly values are presented, the calculations have been made on an hourly basis.
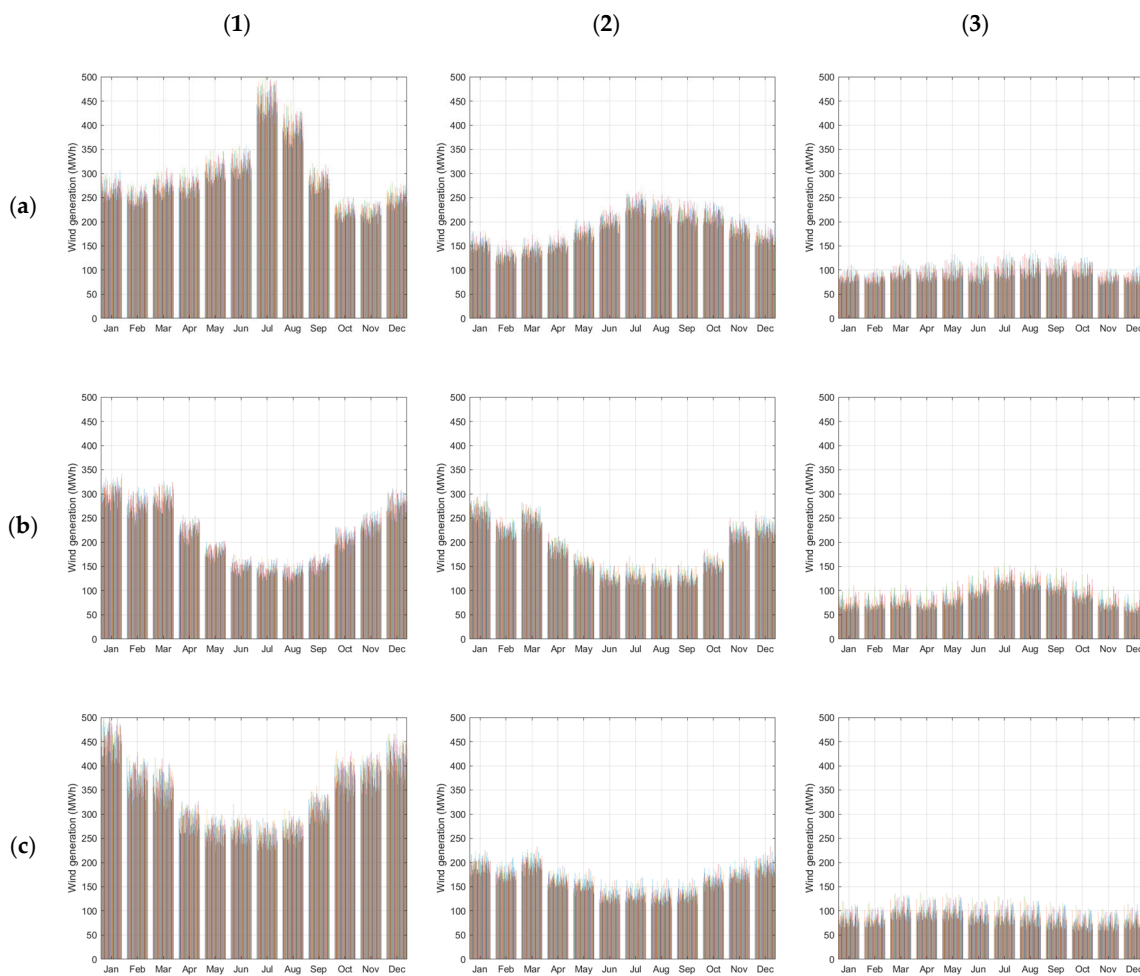
Figure 7. Average monthly wind generation for the nine terrestrial locations considered: (**a**–**c**) solar irradiance: high, moderate, and low; (**1**–**3**) wind speed: high, moderate, and low.
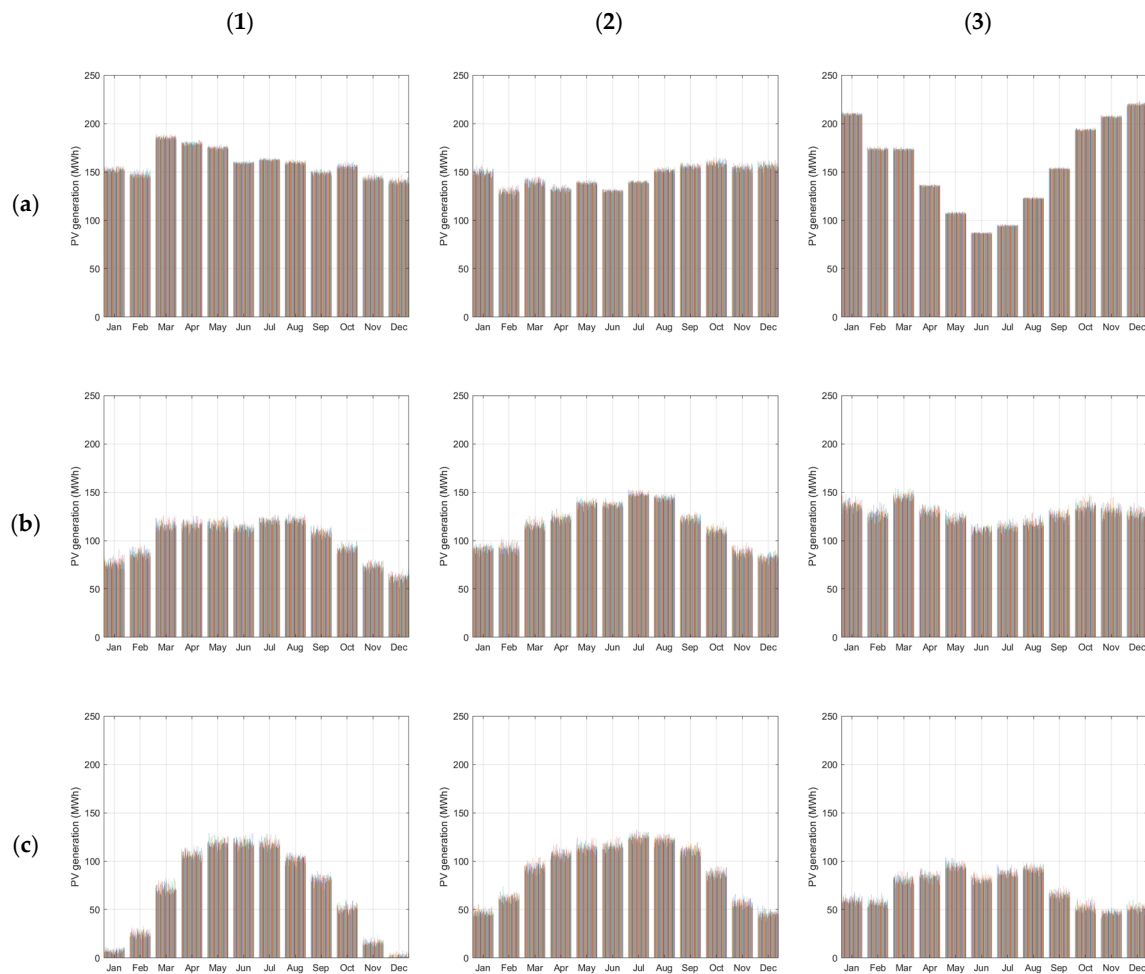
Figure 8. Average monthly solar generation for the nine terrestrial locations considered: (**a**–**c**) solar irradiance: high, moderate, and low; (**1**–**3**) wind speed: high, moderate, and low.

As can be seen in Figure 7, wind generation, if averaged values are analyzed, may seem to have a fairly constant generation throughout the year. With monthly values around 100 MWh for low wind locations (Figure 7-3), around 150–250 for moderate wind locations (Figure 7-2), and between 200 and 350 for high wind locations (Figure 7-1), although even reaching values of almost 500 MWh in the case of the Sahara and North Sea coast. Although, as detailed later, when analyzing hourly values, even more significant differences can be appreciated. On the other hand, the graph clearly shows the differences in generation levels between the high, moderate, and low wind zones, with average capacity factors of around 40%, 25%, and around 15%, respectively (Table 4). Despite this relative stability of the monthly average values for all the simulations, depending on the location, it can be seen that there are differences in generation between different periods of the year. For example, in the coastal Sahara area, there are very high generation values throughout the year (Figure 7(a1)), but the winter months, from November to February, show clearly lower values, while in late spring and early summer there are the highest productions, in May, June, and July. In other sites the differences are not so great, but even so there are usually at least two levels of generation, a lower one around the winter months and a higher one around the summer months.

Table 4. Summary of the main statistical variables for the wind generation in the nine Earth locations.

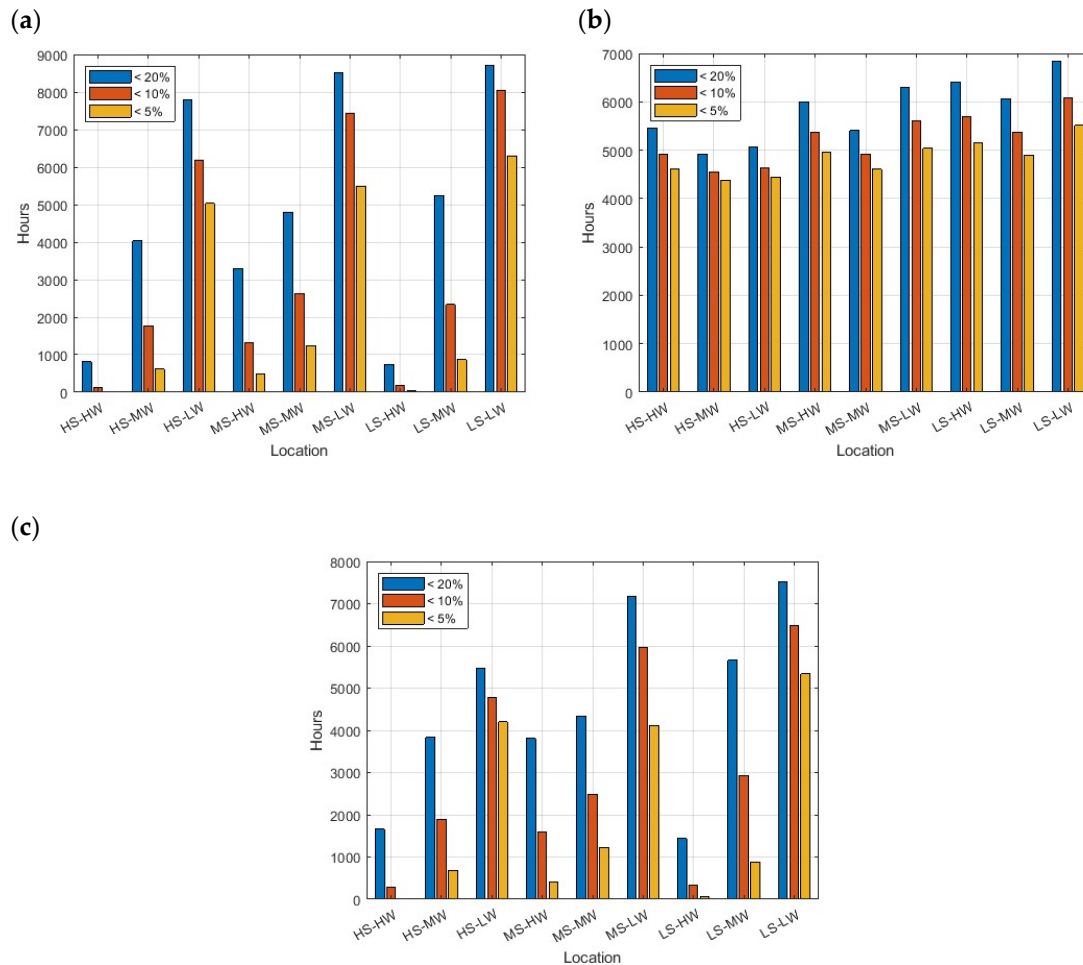| Locations	Generation (MWh)				CF
	Min.	Max.	Mean	Median	
HW-HS	3189	3906	3534	3525	0.403
HW-MS	2305	2908	2608	2620	0.298
HW-LS	3613	4370	4018	4042	0.459
MW-HS	1923	2546	2210	2200	0.252
MW-MS	1907	2512	2201	2200	0.251
MW-LS	1727	2294	1957	1954	0.223
LW-HS	906	1453	1127	1119	0.129
LW-MS	818	1480	1082	1040	0.124
LW-LS	1037	1420	1170	1144	0.134

Regarding solar generation, there are also clear differences between the capacity factors of the three solar PV generation levels, with values around 20, 15, and 10% for high, moderate, and low irradiation zones (Table 5). Additionally, there is usually the previously cited clear difference between summer and winter months (Figure 8), except for those locations with low latitudes, where this generation is more homogeneous. In this line, there are the coastal Sahara and south of Africa areas (Figure 8(a1,a2)) where the radiation remains fairly constant for much of the year (also penalizing the production during the summer months due to the negative effect of high temperatures on the performance of solar panels). The location of the Andean zone of northern Chile (Figure 8(a3)), where irradiation is very high in the summer months (October to March, situation in the southern hemisphere) and quite low in the central winter months, with a high average. As mentioned above, for solar generation, it is important how much is generated and when since there are different periods when generation can be extremely low.

Table 5. Summary of the main statistical variables for solar generation in the nine Earth locations.

Locations	Generation (MWh)				CF
	Min.	Max.	Mean	Median	
HW-HS	1900	1928	1914	1915	0.218
HW-MS	1721	1759	1742	1743	0.199
HW-LS	1873	1887	1880	1880	0.215
MW-HS	1178	1233	1231	1211	0.140
MW-MS	1376	1419	1402	1403	0.160
MW-LS	1492	1579	1536	1536	0.175
LW-HS	806	850	828	827	0.095
LW-MS	1066	1240	1096	1094	0.125
LW-LS	835	883	861	860	0.098

Consequently, the study of these low-generation zones is key in the design of generation mixes with strong contributions of renewable generation; therefore, these aspects are emphasized below. First, it is essential to determine the number of hours with low generation in each location. Figure 9 illustrates the annual hours with generation below the commonly used thresholds for low generation, i.e., 5%, 10%, and 20%. These values are

shown for wind, solar, and the combined generation of both in the nine locations analyzed in this study.

(**a**)

(**b**)

(**c**)

Figure 9. Yearly hours below generation threshold values of 5, 10, and 20% of peak power for the studied resources: (**a**) wind; (**b**) sun; (**c**) both contributions.

For wind generation (Figure 9a), locations with low wind resources experience generation values close to the 20% threshold for almost the entire year. While these values decrease significantly for the 10% and 5% thresholds, they remain extremely high, highlighting the clear unsuitability of wind exploitation in these areas. In locations with moderate and especially high wind resources, the hours of generation below these thresholds are much lower. For regions with moderate wind resources, the 20% threshold corresponds to approximately 50% of the hours in a year, the 10% threshold to around 2000 h, and the 5% threshold to about 500 h. In high-wind areas, these values are approximately 1000, 100, and almost negligible for the 20%, 10%, and 5% thresholds, respectively.

In the case of solar generation (Figure 9b), the differences between regions are much less pronounced (the figure also includes nighttime hours in considering the generation thresholds). Across all locations, the number of hours below the 20% generation threshold ranges from approximately 7000 to 5500 for regions with high, moderate, and low irradiation. When the threshold is reduced to 10%, these figures increase to between 6000 and 5000 h. Further lowering the threshold to 5% results in values between 5500 and 4500 h. These findings suggest that photovoltaic solar generation is generally suitable for exploitation in nearly any location.

The combined generation of wind and solar (Figure 9c) exhibits intermediate behavior but leans more toward the characteristics of wind generation. Since solar generation tends to be relatively consistent across locations and does not exhibit significant performance differences like wind, it is the wind generation that primarily determines whether the thresholds are exceeded.

*3.3. Discussion and Major Findings for Sun and Wind Generation over Earth's Zones*

The occurrence of periods of low renewable production is becoming increasingly important in recent years, given the significant increase in the contribution of renewable generation in different areas, coupled with its intrinsic variability and unpredictability. In fact, this phenomenon is often referred to as Dunkelflaute (DF). This DF can become even more significant if the effects of uncertainty in generation sources and systems are considered. These "dark doldrums" are periods when renewable resources (specifically wind and/or solar power) produce little or negligible energy. Nowadays, there is no clear definition of the phenomenon, as the inherent characteristics of renewable energy production within a day make it complicated to establish a "low productivity" within a day scale. Daily variations in renewable energy production make setting a fixed threshold for low productivity difficult. Night-time periods are a clear but inevitable example of solar power lowering energy production. Many authors state that a DF is defined as a period exceeding 60 min when energy production is below a percentage of the installed capacity. It is below a threshold ranging from 0% to 20% of the installed capacity. This threshold is defined by Li et al. [52] as 10%; Ohlendorf and Schill [53] use more extreme values by establishing the threshold at 2 and 5%, while using 20% as a general standard [54].

Entering into the performance of particular situations, in the case of solar generation, obviously, there will be no generation during the night periods. But coupled with the nighttime periods, there can be very rainy or even just cloudy days leading to low solar generation and even periods of low wind, leading to an extremely low generation of both resources. For example, considering the usual definition of 20% of peak generation to consider the existence of Dunkelflaute, there are prolonged episodes of reduced generation in regions of low solar and wind resources; specifically, in the Sichuan region, there is a period of about 48 h (hours 7479 to 7542) where 20% of solar peak power generation is not reached in any of the hours (Figure 10a). This situation is much more pronounced in the case of wind (Figure 10b), also for this location, where we have had about half a year without exceeding 20% of the peak power (remember that we have the annual hourly performance of 93 simulations randomly sampled through the PDFs found from the historical data used). Therefore, obviously this location would be very unsuitable for the installation of this technology. In this case, given the poor performance of wind generation, the aggregate of the two practically follows the performance of solar generation (Figure 10c).

At the complete opposite point is the coastal area of the Sahara Desert, near the Layoune, where sun and wind present optimal conditions (Figure 11). Even in the case of an optimal region of sun and wind resources, where there is practically no appreciable precipitation and wind conditions are very good, there are quite long periods of low generation. Specifically in the case of solar generation, there has not been a single day that has not reached 20% generation, so that the period of low generation is reduced from the last hours of one day in the afternoon to the first hours of sunshine the following day, just only 19 h (Figure 11a). In the case of wind (Figure 11b), as conditions are also very favorable, there is a very short period of time with generation below 20%, in this case of only 20 h (hours 7206 to 7225). In the case of the consideration of both generations

(Figure 11c), the period of time with low generation is mainly given by the night period, so that we also have an interval very similar to the previous ones, being only 15 h.

If, instead of analyzing the impact of fixing the low-generation threshold at 20%, it is examined how the maximum duration of DF events throughout the year is affected by considering lower threshold values, Figure 12. Naturally, this results in a decrease in DF event duration, with wind generation being most impacted by this change, as solar generation is largely determined by the day–night cycle.
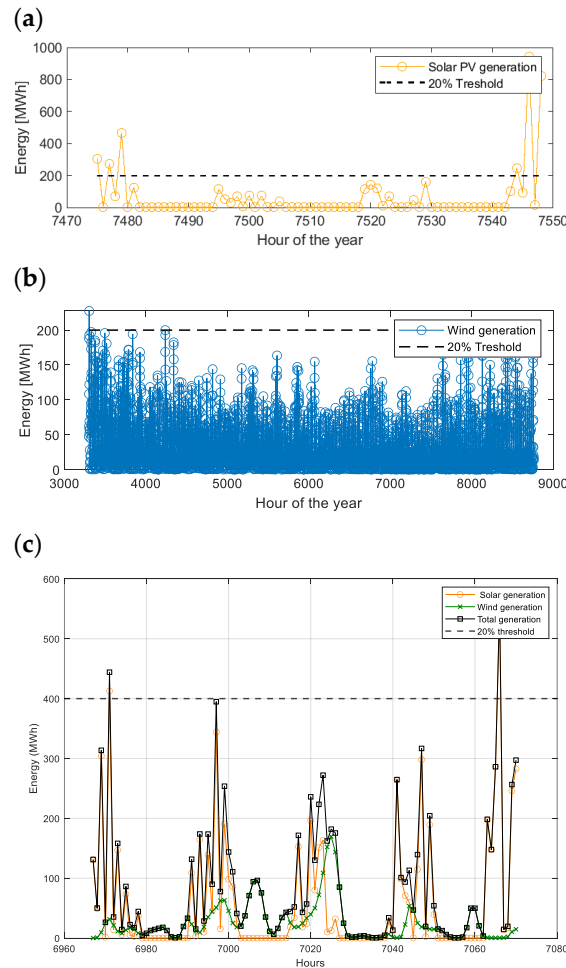
Figure 10. Low-generation periods (DF events) for a region with low radiation and winds: (**a**) solar PV; (**b**) wind; (**c**) both added.

In general, across all locations, the duration of DF events for the solar generation begins at values slightly above 20 h and stabilizes around or slightly below 20 h. Exceptions are found in areas with low solar irradiation (Figure 12c), where these durations are initially higher but also converge to around 20 h for low threshold values. However, wind generation exhibits a much greater sensitivity to the chosen threshold. In locations with high wind resources (Figure 12-1), DF durations can initially exceed 20 h—reaching over 100 h in one case—but they rapidly decrease to just a few hours as the threshold is lowered to approximately 5%. Conversely, in locations with low wind resources (Figure 12-3), DF durations for a 20% threshold reach extremely high values (thousands of hours) but drop quickly with lower thresholds, eventually reaching tens of hours for thresholds around 2%. For locations with moderate wind resources (Figure 12b), DF durations start in the hundreds of hours at the 20% threshold and decrease to around 20 h for thresholds between 2% and 5%.
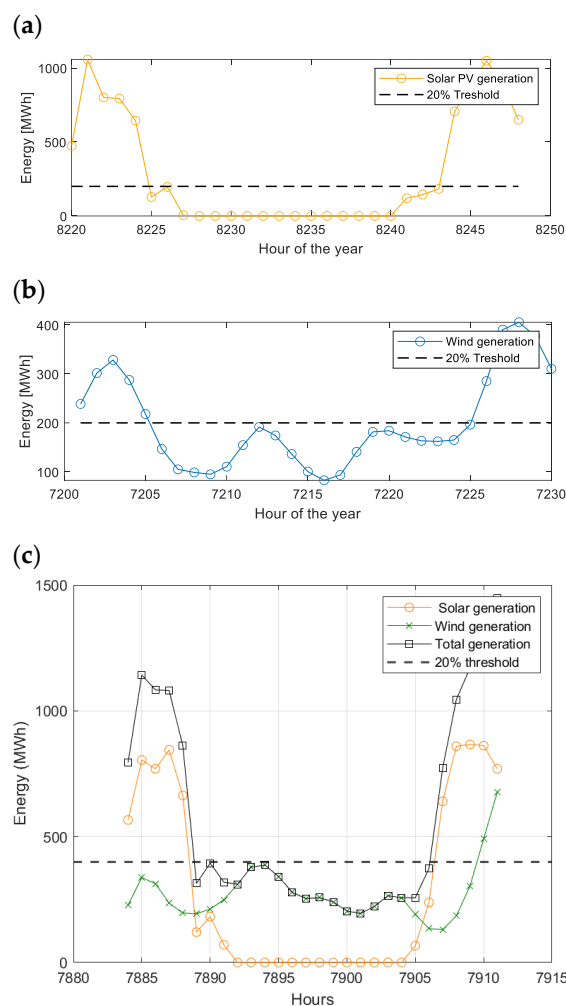
Figure 11. Low generation periods (DF events) for a region with high radiation and winds: (**a**) solar PV; (**b**) wind; (**c**) both added.

When combining both wind and solar resources, the aggregate DF duration generally aligns with the shorter DF duration of the two resources. This is because, in most cases, when one resource's contribution increases, its generation comfortably exceeds the imposed threshold, ensuring that the combined generation surpasses the DF threshold.

As highlighted, locations with low wind resources should generally be excluded from wind energy installations. Their low capacity, coupled with high variability, leads to prolonged periods of low generation, making their exploitation impractical. On the contrary, solar resources can still be viable even in locations with relatively low insolation. Although they result in lower CFs and longer DF durations, these remain manageable. For locations with medium to high levels of both resources, a combination of solar and wind is likely the optimal approach.

However, it is crucial to note that in systems entirely reliant on renewable energy, even the observed DF durations present significant challenges for ensuring energy coverage. If the threshold is set at 20%, this implies that if the demand approaches this 20% threshold, five times the required capacity must be installed. This would lead to overgeneration and consequent electric surpluses during many periods of the year, while during others, generation would not be sufficient, causing possible blackouts if backup generation and/or storage systems to deal with energy shortages were not properly sized.
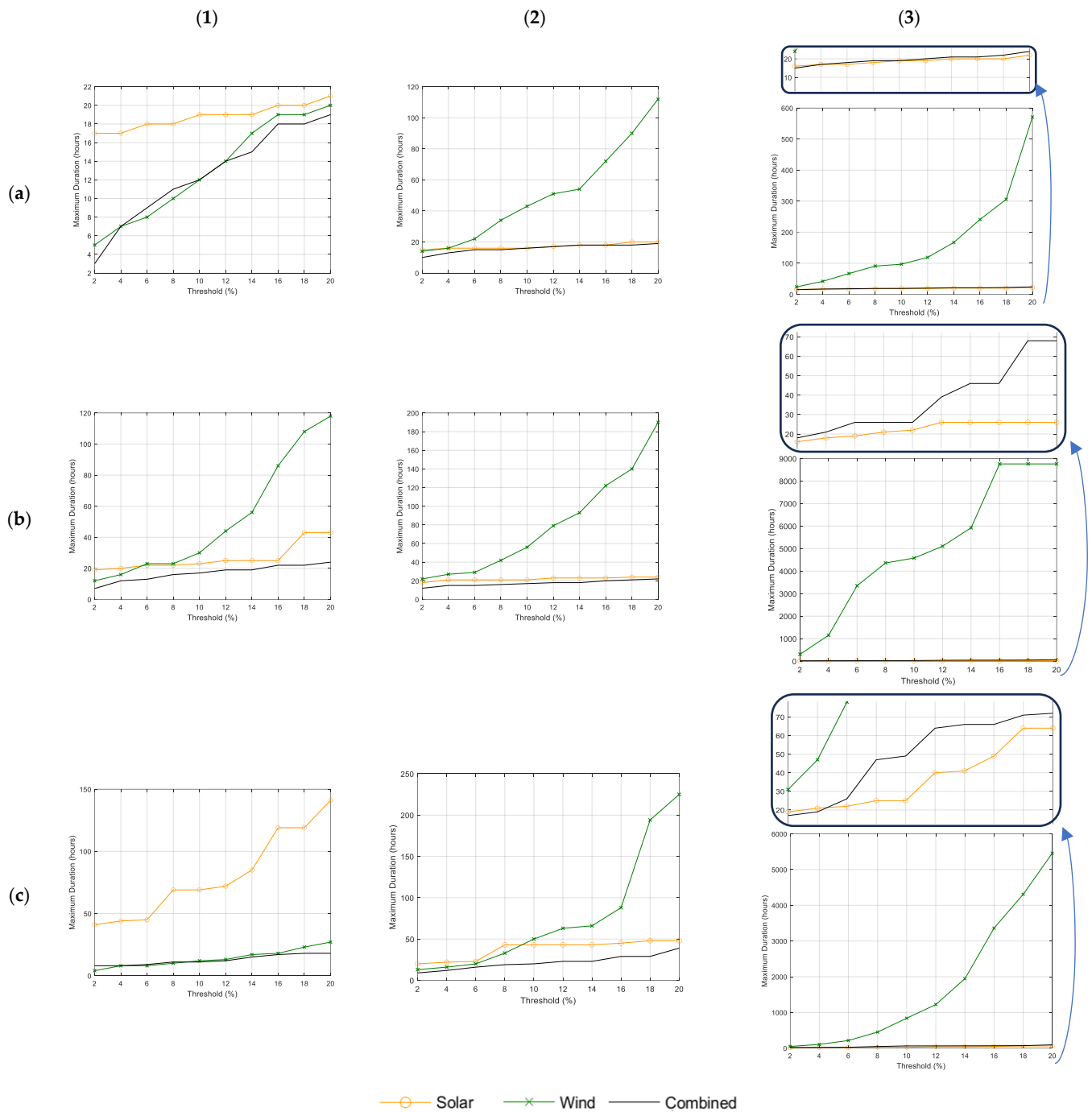
Figure 12. Duration of the maximum DF period as a function of the threshold value for the nine terrestrial locations considered: (**a**–**c**) solar irradiance: high, moderate, and low; (**1**–**3**) wind speed: high, moderate, and low.

Another key consideration is that energy demand is not constant over time. As such, these findings should be viewed as a general reference for system behavior. Measures such as demand-side management (DSM) will be essential to better align generation and consumption, potentially reducing the requirements for backup and storage systems. Overall, this analysis highlights the behavior and evolution of DF events depending on the type of location and the characteristics of the solar and wind resources available in the area.

4. Conclusions

Solar and wind energy are central to achieving net-zero emissions, but their intermittency, unpredictability, and location-dependent nature pose challenges for energy system reliability. The mismatch between renewable generation and electricity demand often necessitates backup fossil-fuel-based power. To address this, probabilistic modeling, particularly Monte Carlo simulations, is used to analyze uncertainties by generating synthetic datasets for wind speed, temperature, and solar irradiance based on 22 years of data. These models employ probability distribution functions (PDFs) to simulate annual renewable energy availability). In the current study, beta is used for solar irradiance, Weibull for wind speed, and normal for temperature. Wilks' formula suggests that 93 simulation runs are sufficient to achieve a 95% confidence level.

Periods of Dunkelflaute (DF), prolonged low renewable energy production, highlight the need for energy storage, demand response, and backup solutions. These critical periods, where renewable generation drops below a set threshold (typically 10–20%), present a major challenge in countries like Germany, which still relies on fossil fuels during winter due to underdeveloped large-scale chemical storage. Addressing DF requires consistent energy mixes, including mainly battery storage and backup solutions, always depending on regional characteristics. However, a location's geographical and climatic characteristics significantly influence the measures taken. High wind-high solar locations benefit from natural complementaries between the two resources. In such regions, like coastal areas or deserts, storage systems might primarily address short-term variability, such as night-time consumption or brief wind calmness. In contrast, inland areas or regions with consistently overcast and low-wind conditions might struggle to meet baseline demand without a combination of long-duration storage, demand-side adjustments, and interconnections to regions with better resource availability.

Future research should prioritize the integration of advanced optimization techniques to enhance the efficiency and reliability of renewable energy deployment. This includes addressing short-term fluctuations through improved forecasting, real-time grid management, and demand-side strategies, as well as tackling long-duration storage challenges with innovative energy storage solutions tailored to location-specific characteristics. An integrative approach that balances economic viability, environmental sustainability, and energy security is essential to ensure a resilient transition toward net-zero emissions. By aligning technological advancements with policy frameworks and investment strategies, the path to sustainable development can be both scalable and adaptable to diverse regional energy needs.

Institutional Review Board Statement: Not applicable.

Informed Consent Statement: Not applicable.

Data Availability Statement: The raw data supporting the conclusions of this article will be made available by the authors on request.

References

1. IEA-International Energy Agency. World Energy Outlook 2023. 2023. Available online: www.iea.org/terms (accessed on 28 January 2025).

2. International Energy Agency. Global Energy Review 2021 Assessing the Effects of Economic Recoveries on Global Energy Demand and CO_2 Emissions. 2021. Available online: https://www.iea.org/reports/global-energy-review-2021 (accessed on 16 December 2024).

3. BP. Energy Outlook 2022 Edition. 2022. Available online: https://www.bp.com/content/dam/bp/business-sites/en/global/corporate/pdfs/energy-economics/energy-outlook/bp-energy-outlook-2022.pdf (accessed on 19 September 2024).

4. UNECE—United Nations Economic Commission for Europe. *Carbon Neutrality in the UNECE Region: Integrated Life-Cycle Assessment of Electricity Sources*; UNECE—United Nations Economic Commission for Europe: Geneva, Switzerland, 2022.

5. Davis, S.J.; Lewis, N.S.; Shaner, M.; Aggarwal, S.; Arent, D.; Azevedo, I.L.; Benson, S.M.; Bradley, T.; Brouwer, J.; Chiang, Y.M.; et al. Net-zero emissions energy systems. *Science* **2018**, *360*, eaas9793. [CrossRef] [PubMed]

6. Whiting, K.; Carmona, L.G.; Sousa, T. A review of the use of exergy to evaluate the sustainability of fossil fuels and non-fuel mineral depletion. *Renew. Sustain. Energy Rev.* **2017**, *76*, 202–211. [CrossRef]

7. Capellán-Pérez, I.; Mediavilla, M.; de Castro, C.; Carpintero, Ó.; Miguel, L.J. Fossil fuel depletion and socio-economic scenarios: An integrated approach. *Energy* **2014**, *77*, 641–666. [CrossRef]

8. Jiang, X.; Guan, D. Determinants of global CO_2 emissions growth. *Appl. Energy* **2016**, *184*, 1132–1141. [CrossRef]

9. Henriques, S.T.; Borowiecki, K.J. The drivers of long-run CO_2 emissions in Europe, North America and Japan since 1800. *Energy Policy* **2017**, *101*, 537–549. [CrossRef]

10. IEA/NEA. Projected Costs of Generating Electricity. 2020. Available online: https://www.iea.org/reports/projected-costs-of-generating-electricity-2020 (accessed on 19 September 2024).

11. Berna-Escriche, C.; Pérez-Navarro, Á.; Escrivá, A.; Hurtado, E.; Muñoz-Cobo, J.L.; Moros, M.C. Methodology and application of statistical techniques to evaluate the reliability of electrical systems based on the use of high variability generation sources. *Sustainability* **2021**, *13*, 10098. [CrossRef]

12. Qu, X.; Zhao, G.; Wang, J. Thermodynamic evaluation of hydrogen and electricity cogeneration coupled with very high temperature gas-cooled reactors. *Int. J. Hydrogen Energy* **2021**, *46*, 29065–29075. [CrossRef]

13. Capros, P.; Kannavou, M.; Evangelopoulou, S.; Petropoulos, A.; Siskos, P.; Tasios, N.; Zazias, G.; DeVita, A. Outlook of the EU energy system up to 2050: The case of scenarios prepared for European Commission's "clean energy for all Europeans" package using the PRIMES model. *Energy Strat. Rev.* **2018**, *22*, 255–263. [CrossRef]

14. Rivera, Y.; Blanco, D.; Bastida-Molina, P.; Berna-Escriche, C. Assessment of a Fully Renewable System for the Total Decarbonization of the Economy with Full Demand Coverage on Islands Connected to a Central Grid: The Balearic Case in 2040. *Machines* **2023**, *11*, 782. [CrossRef]

15. Berna-Escriche, C.; Vargas-Salgado, C.; Alfonso-Solar, D.; Escrivá-Castells, A. Hydrogen Production from Surplus Electricity Generated by an Autonomous Renewable System: Scenario 2040 on Grand Canary Island, Spain. *Sustainability* **2022**, *14*, 11884. [CrossRef]

16. Rivera-Durán, Y.; Berna-Escriche, C.; Córdova-Chávez, Y.; Muñoz-Cobo, J.L. Assessment of a Fully Renewable Generation System with Storage to Cost-Effectively Cover the Electricity Demand of Standalone Grids: The Case of the Canary Archipelago by 2040. *Machines* **2023**, *11*, 101. [CrossRef]

17. United Nations. The Paris Agreement. 2023. Available online: https://unfccc.int/process-and-meetings/the-paris-agreement (accessed on 21 August 2023).

18. European Commission. Strategic Energy Technology Plan. 2023. Available online: https://energy.ec.europa.eu/topics/research-and-technology/strategic-energy-technology-plan_en (accessed on 21 July 2024).

19. European Commission. *Implementing the Repower EU Action Plan: Investment Needes, Hydrogen Accelerator and Achieving the Bio-Methane Targets (REPowerEU Plan)*; European Commission: Brussels, Belgium, 2022.

20. Berna-Escriche, C.; Rivera-Durán, Y.; Córdova-Chávez, Y.; Muñoz-Cobo, J.L. Maximizing the use of hydrogen as energy vector to cover the final energy demand for stand-alone systems, application and sensitivity analysis for the Canary Archipelago by 2040. *Prog. Nucl. Energy* **2023**, *163*, 104791. [CrossRef]

21. Monitor Deloitte. *Una Transición Inteligente Hacia un Modelo Energético Sostenible Para España en 2050: La Eficiencia Energética y la Electrificación*; Monitor Deloitte: London, UK, 2018.

22. Dellano-Paz, F.; Calvo-Silvosa, A.; Antelo, S.I.; Soares, I. The European low-carbon mix for 2030: The role of renewable energy sources in an environmentally and socially efficient approach. *Renew. Sustain. Energy Rev.* **2015**, *48*, 49–61. [CrossRef]

23. Tong, D.; Farnham, D.J.; Duan, L.; Zhang, Q.; Lewis, N.S.; Caldeira, K.; Davis, S.J. Geophysical constraints on the reliability of solar and wind power worldwide. *Nat. Commun.* **2021**, *12*, 6146. [CrossRef] [PubMed]

24. Ahmad, T.; Zhang, H.; Yan, B. A review on renewable energy and electricity requirement forecasting models for smart grid and buildings. *Sustain. Cities Soc.* **2020**, *55*, 102052. [CrossRef]

25. Williams, S.; Short, M. Electricity demand forecasting for decentralised energy management. *Energy Built Environ.* **2020**, *1*, 178–186. [CrossRef]

26. Rubel, F.; Kottek, M. Observed and projected climate shifts 1901-2100 depicted by world maps of the Köppen-Geiger climate classification. *Meteorol. Z.* **2010**, *19*, 135–141. [CrossRef]

27. Mazzeo, D.; Matera, N.; De Luca, P.; Baglivo, C.; Congedo, P.M.; Oliveti, G. Worldwide geographical mapping and optimization of stand-alone and grid-connected hybrid renewable system techno-economic performance across Köppen-Geiger climates. *Appl. Energy* **2020**, *276*, 115507. [CrossRef]

28. Ascencio-Vásquez, J.; Brecl, K.; Topič, M. Methodology of Köppen-Geiger-Photovoltaic climate classification and implications to worldwide mapping of PV system performance. *Sol. Energy* **2019**, *191*, 672–685. [CrossRef]

29. Solaun, K.; Cerdá, E. Climate change impacts on renewable energy generation. A review of quantitative projections. *Renew. Sustain. Energy Rev.* **2019**, *116*, 109415. [CrossRef]

30. NASA. Data Access Viewer. 2024. Available online: https://power.larc.nasa.gov/data-access-viewer/ (accessed on 20 May 2024).

31. Kondziella, H.; Specht, K.; Lerch, P.; Scheller, F.; Bruckner, T. The techno-economic potential of large-scale hydrogen storage in Germany for a climate-neutral energy system. *Renew. Sustain. Energy Rev.* **2023**, *182*, 113430. [CrossRef]

32. Meschede, H.; Hesselbach, J.; Child, M.; Breyer, C. On the impact of probabilistic weather data on the economically optimal design of renewable energy systems—A case study of la gomera island. *Int. J. Sustain. Energy Plan. Manag.* **2019**, *23*, 15–26. [CrossRef]

33. Wilks, S.S. Determination of sample sizes for setting tolerance limits. *Ann. Math. Stat.* **1941**, *12*, 91–96. [CrossRef]

34. Wilks, S.S. Statistical prediction with special reference to the problem of tolerance limits. *Ann. Math. Stat.* **1942**, *13*, 400–409. [CrossRef]

35. Wald, A. An extension of wilks' method for setting tolerance limits. *Ann. Math. Stat.* **1943**, *14*, 45–55. [CrossRef]

36. Glaeser, H. GRS method for uncertainty and sensitivity evaluation of code results and applications. *Sci. Technol. Nucl. Install.* **2008**, *2008*, 798901. [CrossRef]

37. Alzbutas, R.; Norvaisa, E. Uncertainty and sensitivity analysis for economic optimisation of new energy source in Lithuania. *Prog. Nucl. Energy* **2012**, *61*, 17–25. [CrossRef]

38. Álvarez-Piñeiro, L.; Rivera, Y.; Berna-Escriche, C.; Blanco, D. Formulation of best estimate plus uncertainty methodologies for economy decarbonization in high-energy-demand isolated systems: Canary Islands forecasts for 2040. *Energy Convers. Manag.* **2024**, *314*, 118691. [CrossRef]

39. Berna-Escriche, C.; Rivera, Y.; Alvarez-Piñeiro, L.; Muñoz-Cobo, J.L. Best estimate plus uncertainty methodology for forecasting electrical balances in isolated grids: The decarbonized Canary Islands by 2040. *Energy* **2024**, *294*, 130801. [CrossRef]

40. European Commission. *Photovoltaic Geographical Information System (PVGIS)*; European Commission: Brussels, Belgium, 2022.

41. Fatemi, S.A.; Kuh, A.; Fripp, M. Parametric methods for probabilistic forecasting of solar irradiance. *Renew. Energy* **2018**, *129*, 666–676. [CrossRef]

42. Seguro, J.V.; Lambert, T.W. Modern estimation of the parameters of the Weibull wind speed distribution for wind energy analysis. *J. Wind. Eng. Ind. Aerodyn.* **2000**, *85*, 75–84. [CrossRef]

43. Gubler, S.; Fukutome, S.; Scherrer, S.C. On the statistical distribution of temperature and the classification of extreme events considering season and climate change—an application in Switzerland. *Theor. Appl. Clim.* **2023**, *153*, 1273–1291. [CrossRef]

44. Keddouda, A.; Ihaddadene, R.; Boukhari, A.; Atia, A.; Arıcı, M.; Lebbihiat, N.; Ihaddadene, N. Solar photovoltaic power prediction using artificial neural network and multiple regression considering ambient and operating conditions. *Energy Convers. Manag.* **2023**, *288*, 117186. [CrossRef]

45. Duffie, J.A.; Beckman, W.A. *Solar Engineering of Thermal Processes*; Wiley: Hoboken, NJ, USA, 2013.

46. Pantic, L.S.; Pavlović, T.M.; Milosavljević, D.D.; Radonjic, I.S.; Radovic, M.K.; Sazhko, G. The assessment of different models to predict solar module temperature, output power and efficiency for Nis, Serbia. *Energy* **2016**, *109*, 38–48. [CrossRef]

47. Langner, F.; Wang, W.; Frahm, M.; Hagenmeyer, V. Model predictive control of distributed energy resources in residential buildings considering forecast uncertainties. *Energy Build.* **2023**, *303*, 113753. [CrossRef]

48. Letzgus, S.; Müller, K.R. An explainable AI framework for robust and transparent data-driven wind turbine power curve models. *Energy AI* **2024**, *15*, 100328. [CrossRef]

49. Bobtsov, A.; Ortega, R.; Aranovskiy, S.; Cisneros, R. On-line estimation of the parameters of the windmill power coefficient. *Syst. Control. Lett.* **2022**, *164*, 105242. [CrossRef]

50. Bustos-Turu, G. Comparison of Fixed Speed Wind Turbines Models: A Case Study. In Proceedings of the IECON 2013-39th Annual Conference of the IEEE Industrial Electronics Society, Vienna, Austria, 10–14 November 2013.

51. Bustos, G.; Vargas, L.S.; Milla, F.; Saez, D.; Zareipour, H.; Nunez, A. Comparison of fixed speed wind turbines models: A case study. In Proceedings of the 38th Annual Conference on IEEE Industrial Electronics Society, Montreal, QC, Canada, 25–28 October 2012; pp. 961–966. [CrossRef]

52. Li, B.; Basu, S.; Watson, S.J.; Russchenberg, H.W.J. Mesoscale modeling of a "Dunkelflaute" event. *Wind. Energy* **2021**, *24*, 5–23. [CrossRef]

53. Ohlendorf, N.; Schill, W.P. Frequency and duration of low-wind-power events in Germany. *Res. Lett.* **2020**, *15*, 084045. [CrossRef]

54. Sabovčík, R.; Hradický, J.M.; Šinka, M. Leveraging open-source data to study solar-wind complementarity in the global perspective. *Renew. Energy Focus* **2024**, *50*, 100583. [CrossRef]